Journal of Sound and Vibration 442 (2019) 237–248

Contents lists available at ScienceDirect

Journal of Sound and Vibration

journal homepage: www.elsevier.com/locate/jsvi

Tailoring vibration suppression bands with hierarchical metamaterials containing local resonators

Xianchen Xu, Miles V. Barnhart, Xiaopeng Li, Yangyang Chen*, Guoliang Huang**

Department of Mechanical and Aerospace Engineering, University of Missouri, Columbia, MO, 65211, USA

ARTICLE INFO

Article history:
Received 29 April 2018
Received in revised form 28 October 2018
Accepted 30 October 2018
Available online 2 November 2018
Handling Editor: D. Juve

Keywords:
Hierarchical metamaterial
Inner-resonance
Broadband attenuation

ABSTRACT

Vibration suppression at subwavelength scales is of great interest in acoustic and/or elastic metamaterial engineering which has a wide range of potential applications requiring dynamic stabilities by using light-weight structures and materials. In this study, we propose the concept of metamaterials with hierarchically organized local resonators, which possess the ability to efficiently tailor elastic wave or vibration attenuation to various frequency regions through different hierarchical designs. Wave dispersion relations and band gap behaviors of one-dimensional lumped mass-spring hierarchical metamaterials are characterized first with outward and inward hierarchical configurations. A honeycomb hierarchical lattice with embedded rubber-coated lead cylinders is then designed to demonstrate the vibration suppression at subwavelength scales in two separate frequency regions, where the first-order outward hierarchy is selected. Good agreement between experimental and numerical results are clearly observed in the frequency response functions of a metamaterial sample. The hierarchical metamaterials are demonstrated to be efficiency solutions in elastic wave bandgap engineering at subwavelength scales, which will benefit light-weight passive structures for low-frequency vibration and/or elastic wave mitigation.

1. Introduction

In recent years, a great deal of research has been conducted on acoustic/elastic metamaterials exhibiting unusual dynamic effective material properties produced by artificially engineered microstructures [1–5]. The primary components in the design of metamaterials are locally resonant inclusions at subwavelength scales such that the acoustic/elastic metamaterial can be regarded as an effective continuum media exhibiting, for example, negative effective mass density and/or negative effective moduli [6–12]. The design approach based on the local resonance mechanism sheds new light on the low-frequency mechanical wave and/or vibration attenuation with compelling advantages compared with conventional approaches, where large or heavy materials/structures are usually involved. Some novel applications of metamaterials include noise and sound treatment, underwater acoustics, structural vibration suppression, earthquake protection, negative refraction, imaging, lensing and cloaking [13–21]. However, the wave propagation band gaps induced by local resonances of conventional

* Corresponding author.
** Corresponding author.
E-mail addresses: yc896@mail.missouri.edu (Y. Chen), huangg@missouri.edu (G. Huang).

https://doi.org/10.1016/j.jsv.2018.10.065
0022-460X/

metamaterials are usually narrow and fixed, which is a fundamental challenge in the development of acoustic/elastic metamaterials.

To enhance the band gap formation behavior and tailor the wave attenuation regions of metamaterials over broader frequencies, many approaches have been suggested by adopting either passive or active design aspects. Integrating multiple or gradient resonators into a host medium is one of the most widely used strategies to enlarge wave/vibration attenuation frequency regions in a structure [22]. Other common passive strategies include utilization of material dissipation and/or nonlinear properties [23–29] by balancing material damping and/or nonlinearities with resonances. On the other hand, tunable or adaptive resonators built with shunted piezoelectric materials have also been suggested in active metamaterials to achieve broadband wave attenuation [30–38]. However, the damping or nonlinear coefficients required for broadband applications are usually extreme values, which cannot be easily found in natural materials, and active approaches usually require complex control circuits and have stability issues. Therefore, finding a convenient and cost-efficient way to incorporate multiple resonators to stabilize light-weight metamaterial microstructures with relatively high-quasi-static-strength at broadband frequencies is of practical importance in various engineering problems, ranging from biological engineering at nano/micro-meter scales to civil engineering at meter scales.

It is well known that many biological structural materials have superior mechanical properties over some high-performance synthetic materials [39–41], i.e. the Bombardier Beetle's explosion chamber possesses high impact tolerance [42] and strong vibration damping is provided by the woodpecker skull [43]. Previous investigations have suggested that hierarchical structures are responsible for those properties [44–46]. Inspired by this, several hierarchical metamaterials with broadband vibration and acoustic mitigation capabilities [47–52], exceptional wave attenuation at multiband frequencies [53,54] and new bio-inspired designs for Bragg gap generation [55] have recently been reported. To this end, hierarchical lattice metamaterials, such as hexagonal, Kagome, triangular and honeycomb lattices, have been widely employed in a range of studies, because they are light-weight and have relatively high-stiffness and high energy absorption capability. Honeycomb structures, in particularly, have been extensively studied in recent years due to their inherent structural stability [43]. Mousanezhad et al. recently investigated the propagation of two-dimensional (2D) elastic waves in a sandwiched hexagonal lattice structure possessing a two-order hierarchy [49]. Although it provided early evidence of bandgap formation in hierarchical honeycomb structures, this study seems to overlook the mechanisms controlling the opening of stopping bands and how they can be tuned by specifically designed boundary conditions. It should also be noted that previous studies of hierarchical lattice metamaterials on wave vibration attenuation are all based on Bragg scattering at relatively high-frequencies while studies on hierarchical lattice metamaterials with local resonators for relatively low-frequency wave/vibration attenuation at subwavelength scales remain very few.

In this study, we propose hierarchical metamaterials with embedded local resonators and numerically and experimentally demonstrate the low-frequency vibration suppression at two separate frequency bands of a honeycomb lattice with hierarchically organized resonators at subwavelength scales. This work is organized as follows: in Section 2, the hierarchical metamaterial with resonators is simplified as a one-dimensional (1D) lumped mass-spring lattice system and classified into two configurations where resonators are attached according to either an inward or outward hierarchical order. Wave dispersion relations of the two configurations are then characterized by a developed analytical model. In Section 3, the hierarchical honeycomb lattice metamaterial (HHM) with outward first-order hierarchy is designed for desired broadband wave attenuation at subwavelength scales, and dispersion diagrams are simulated numerically for the lattices with and without resonators. Meanwhile, the experimental testing on the vibration suppression of the lattice design is performed where good agreement between experimental and numerical results are observed. In Section 4, a summary of this work is provided.

2. 1D lumped mass-spring lattice with hierarchical resonators

2.1. Modeling of the 1D lumped mass-spring lattice

Locally resonant elastic metamaterials have been extensively studied based on lumped mass-spring lattice systems including the cases containing both single and multiple resonators [19,25,29,56,57]. Wave dispersion relations and effective material parameters have been obtained with satisfactory accuracies compared with the continuous modeling for a range of designs. Here, we begin our studies by considering a 1D lumped mass-spring lattice system with hierarchically arranged multiple resonators. Investigating these simple representations of hierarchical metamaterials could easily unveil the mechanisms in wave band gap control by using different hierarchies, inward or outward, and provide general design guidelines for real structural implementations.

Fig. 1 shows the schematic of the 1D lumped metamaterial with hierarchically outward (Fig. 1(a)) and inward resonators (Fig. 1(b)). In the following expressions, the superscripts "$^{(I)}$" and "$^{(O)}$" denote the outward and inward configurations, respectively. As shown in the figure, the outer masses ($m_0^{(O)}$ and $m_0^{(I)}$) of the two lattices are interconnected with springs of constants $k_0^{(O)}$ and $k_0^{(I)}$, respectively. For the outward configuration (Fig. 1(a)), all inner masses, $m_i^{(O)} (i = 1, 2, \ldots, n)$ are at the same level and directly connected to the outermost mass with inner springs, $k_i^{(O)} (i = 1, 2, \ldots, n)$, respectively. In contrast, the inward configuration shown in Fig. 1(b) is a genuine hierarchical configuration where the resonators with masses, $m_i^{(I)} (i = 1,$

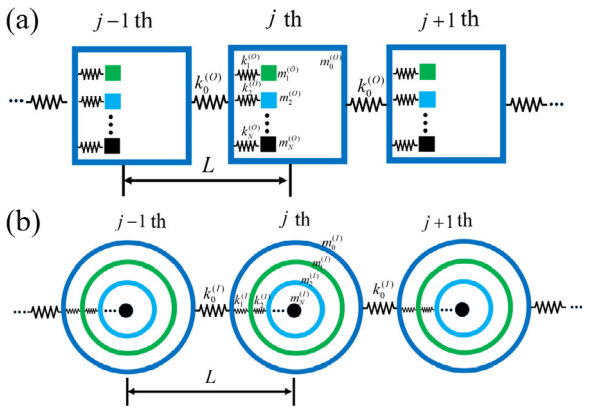

Fig. 1. Schematic of one-dimensional mass-spring lattices for (a) outward and (b) inward hierarchical configurations.

2, …, n) and inner springs, $k_i^{(I)}$ ($i = 1, 2, \ldots, n$) are imbricated one into the other. The hierarchical order of the lattice system is defined as $N - 1$, where N is the number of total resonators in the unit cell of the lattice system.

For the outward configuration, the equations of motion for the j-th unit cell can be written as

$$m_0^{(O)}\frac{d^2u_0^{(j)}}{dt^2} + k_0^{(O)}\left(2u_0^{(j)} - u_0^{(j-1)} - u_0^{(j+1)}\right) + \sum_{n=1}^{N} k_n^{(O)}\left(u_0^{(j)} - u_n^{(j)}\right) = 0, \tag{1}$$

$$m_n^{(O)}\frac{d^2u_n^{(j)}}{dt^2} + k_n^{(O)}\left(u_n^{(j)} - u_0^{(j)}\right) = 0 \ (n = 1, 2, \ldots, N), \tag{2}$$

where u_n^j represents the displacement of the inner mass number "n" in the j-th unit cell of the lattice. The harmonic wave solution for the $(j + n)$-th unit cell can be assumed in the form [19]

$$u_0^{(j+n)} = B_0 e^{i(jqL + nqL - \omega t)} \ (n = 1, 2, \ldots, N) \tag{3}$$

where B_0 is the complex wave amplitude, q is the wave number and ω is the angular frequency. The substitution of Eq. (3) into Eqs. (1) and (2) yields N homogeneous equations for B_n that combine to form a system of equations written as

$$\begin{bmatrix} 2k_0^{(O)}(1 - \cos qL) + \sum_{i=1}^{n} k_i^{(O)} - m_0^{(O)}\omega^2 & -k_1^{(O)} & -k_2^{(O)} & \cdots & -k_n^{(O)} \\ -k_1^{(O)} & k_1^{(O)} - m_1^{(O)}\omega^2 & 0 & \ddots & 0 \\ -k_2^{(O)} & 0 & \ddots & \ddots & \vdots \\ \vdots & \ddots & \ddots & k_{n-1}^{(O)} - m_{n-1}^{(O)}\omega^2 & 0 \\ -k_n^{(O)} & 0 & \cdots & 0 & k_n^{(O)} - m_n^{(O)}\omega^2 \end{bmatrix} \begin{pmatrix} B_0 \\ B_1 \\ \vdots \\ B_{n-1} \\ B_n \end{pmatrix} = \begin{pmatrix} 0 \\ 0 \\ \vdots \\ 0 \\ 0 \end{pmatrix}, \tag{4}$$

Then, a nontrivial solution exists if and only if the determinant of the system given in Eq. (4) is equal to zero.

In comparison, for the inward configuration, the equations of motion for the j-th unit cell are written as

$$m_0^{(I)}\frac{d^2v_0^{(j)}}{dt^2} + k_0^{(I)}\left(2v_0^{(j)} - v_0^{(j-1)} - v_0^{(j+1)}\right) + k_1^{(I)}\left(v_0^{(j)} - v_1^{(j)}\right) = 0, \tag{5}$$

$$m_n^{(I)}\frac{d^2v_n^{(j)}}{dt^2} + k_n^{(I)}\left(v_n^{(j)} - v_{n-1}^{(j)}\right) + k_{n+1}^{(I)}\left(v_n^{(j)} - v_{n+1}^{(j)}\right) = 0 \ (n = 1, 2, \cdots, N) \tag{6}$$

The substitution of the harmonic wave solution into Eqs. (5) and (6) once again yields N homogeneous equations for the amplitudes B_n given by

$$\begin{bmatrix} 2k_0^{(I)}(1-\cos qL)+k_1^{(I)}-m_0^{(I)}\omega^2 & -k_1^{(I)} & 0 & \cdots & 0 \\ -k_1^{(I)} & k_1^{(I)}+k_2^{(I)}-m_1^{(I)}\omega^2 & -k_2^{(I)} & \ddots & \vdots \\ 0 & -k_2^{(I)} & \ddots & \ddots & 0 \\ \vdots & \ddots & \ddots & k_{n-1}^{(I)}+k_n^{(I)}-m_{n-1}^{(I)}\omega^2 & -k_n^{(I)} \\ 0 & \cdots & 0 & -k_n^{(I)} & k_n^{(I)}-m_n^{(I)}\omega^2 \end{bmatrix} \begin{pmatrix} B_0 \\ B_1 \\ \vdots \\ B_{n-1} \\ B_n \end{pmatrix} = \begin{pmatrix} 0 \\ 0 \\ \vdots \\ 0 \\ 0 \end{pmatrix}. \tag{7}$$

According to Eq. (4) or (7), wave dispersion diagrams of lattice metamaterials containing either inward or outward hierarchies can be determined with given wavenumbers or frequencies.

2.2. Tailoring wave band gaps with hierarchical metamaterials

Zeroth-order inward and outward hierarchical metamaterials will be reduced to the same regular mass-in-mass lattice system that has been extensively studied [14] as shown in Fig. 2(a). By adopting material parameter selections such as, $m_1/m_0 = 4, k_1/k_0 = 4/30$, and $k_0/m_0 = 5\times10^8$ (rad/s)^2, the dispersion relations and effective mass density of the zeroth-order metamaterial are calculated analytically and shown in Fig. 2(b) and (c), respectively. In the figure, the frequencies $\Omega = \omega/\omega_0$, are normalized with respect to the natural frequency of the inner resonator given as $\omega_0 = \sqrt{k_1/m_1}$. As expected, only one bandgap is observed from $\Omega \approx 0.077$ to 0.174 due to the local resonance, where the effective mass is found to be negative as highlighted in Fig. 2(b) and (c).

When the hierarchical order of the metamaterial becomes greater than zero, multiple wave band gaps would occur due to the presence of multiple resonances. Here, the inward and outward hierarchical constructions will produce different band gap frequency regions as the topologies are different. The first examples are the first-order inward and outward hierarchical metamaterials shown in Fig. 3(a) and (b), respectively, where $m_1/m_0 = 3,\ m_2/m_0 = 1,\ k_1/k_0 = 4/30, k_2/k_0 = 4/30, k_0/m_0 = 5\times10^8$ (rad/s)^2. The dispersion diagrams of the outward and inward configurations are shown in Fig. 3(c) and (d), respectively, where two band gaps are clearly seen in both figures. It has already been shown that, for the outward configuration (Fig. 3(c)), the band gap at lower frequencies (from 0.089 to 0.121) is much narrower than that at higher frequencies (from 0.154 to 0.256). Moreover, because the two resonators are separated in geometry without any interactions on the resonant frequencies, the starting frequencies of the two band gaps are almost identical with the resonant frequencies of the two individual resonators. Nevertheless, the band gap widths are determined by the mass and stiffness ratios between resonators, which will be discussed hereafter. For the inward configuration (Fig. 3(d)), the band gap at higher frequencies (from 0.185 to 0.2) is much narrower than that at lower frequencies (from 0.0745 to 0.156). Due to the fact that the two resonators are interconnected in the inward configuration, the resonant frequencies of the resonators are no longer the same as their individual ones. The band gap starting frequencies are therefore determined by the coupling between those two resonators, which are a little bit lower than that of the outward configuration. As a result, the band gaps of the inward configuration

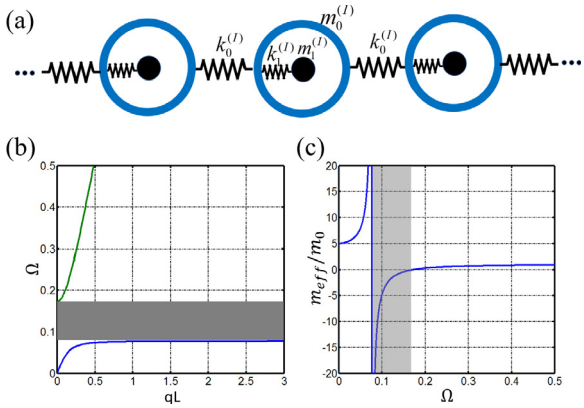

Fig. 2. (a) One-dimensional models for regular metamaterials, (b) dispersion curves of regular inward and outward HHMs, (c) effective mass of regular hierarchies (for regular structure the model for inward HHM is the same as the outward HHM).

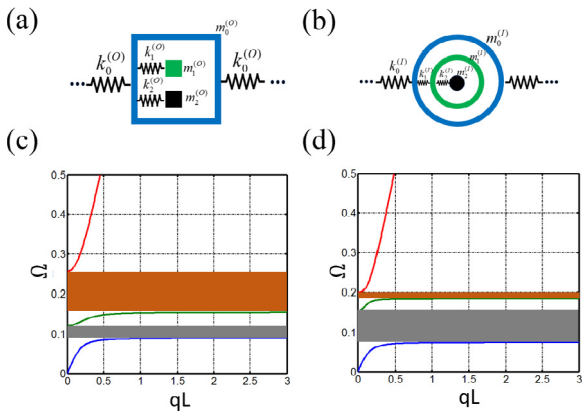

Fig. 3. (a) First order outward HHM, (b) first-order inward HHM, (c) dispersion curve of first-order outward HHM, (d) dispersion curve of first-order of inward HHM.

occupy lower frequencies compared with the band gaps of the outward configuration. When designing band gap locations of an inward hierarchical metamaterial, inner resonators should be considered as a whole.

To further address band gap tailoring abilities provided by outward and inward hierarchical metamaterials with the first-order, resonant band gap frequencies are calculated analytically and shown in Fig. 4 with different mass and stiffness variation factors, α and β. Here, the total mass of a single unit cell is kept as $5m_0^{(o)}$ ($m_0^{(o)} = m_0^{(i)}$) and the mass variation factor, α, is defined as $\alpha = m_2^{(o)}/m_0^{(o)} = m_2^{(i)}/m_0^{(i)}$ and the stiffness variation factor $\beta = k_2^{(o)}/k_0^{(o)} = k_2^{(I)}/k_0^{(I)}$. In the figures, the color regions denote the frequencies where the band gaps occupied. Specifically, the band gaps at lower frequencies are represented by blue regions, and the band gaps at higher frequencies are represented by red regions. The band gap frequencies of outward hierarchical metamaterials with different mass variations are shown in Fig. 4(a) – (c), where $\beta = 2/15$, and $k_1^{(o)}$ is selected as $4k_2^{(o)}$, $k_2^{(o)}$ and $0.25k_2^{(o)}$ in the three figures, respectively. When α is equal to 0 or 4, the first-order outward hierarchical metamaterial is reduced to a zeroth-order metamaterial with only one resonator such that one band gap appears at lower frequencies. Another special situation is that the resonant frequencies of the two resonators are the same, i.e. $\alpha = 2$ in Fig. 4(b), where the two resonators behave as a single resonator effectively and produce only one band gap. This point can be regarded as a mode interchange point. It has already mentioned that the band gap lower-edge frequencies of outward hierarchical metamaterials are independently controlled by the resonant frequencies of individual resonators. Therefore, for the cases with $\alpha < 2$ in Fig. 4(b), the lower-frequency band gap is mainly caused by the out-of-phase motion of m_1 and the higher-frequency band gap is dominated by the out-of-phase motion of $m_2^{(o)}$. When α gradually increases from 0 to 2, the bandwidth of the blue region shrinks to 0, whereas the bandwidth of the red region becomes broader from zero width. The combination effects from the two resonators on the bandwidth control becomes very strong, when α is close to 2, where the low-frequency band gap is very narrow ($m_1^{(o)}$ is out-of-phase and $m_2^{(o)}$ is in-phase), whereas the high-frequency band gap is very broad due to out-of-phase motions of both masses. Furthermore, it should be noted that the band gaps can be tailored to extremely high- and low-frequencies simultaneously with a α near zero. On the other hand, for the cases with $\alpha > 2$, beyond the mode interchange point in Fig. 4(b), the band gap behavior is exactly the same as those with $\alpha < 2$ by just switching the orders of $m_1^{(o)}$ and $m_2^{(o)}$. The band gap tuning phenomenon and mechanism of outward hierarchical metamaterials shown in Fig. 4(a) and (c) are similar with those in Fig. 4(b). The difference is the bias of the mode interchange point to smaller or larger values of α, due to the inner stiffness variations. It is also noticed from Fig. 4(a) – (c) that by increasing the stiffness, $k_1^{(o)}$, the band gaps tend to occupy higher frequencies. The band gap frequencies of inward hierarchical metamaterials with different mass variations are shown in Fig. 4(d) – (f), where $\beta = 2/15$, and $k_1^{(i)}$ is selected as $4k_2^{(I)}$, $k_2^{(I)}$ and $0.25k_2^{(I)}$, respectively, to be the same with that of the outward hierarchical metamaterials demonstrated in Fig. 4(a) – (c). It can be found from the figures that the mode interchange points in Fig. 4(d) – (f) disappear, due to the coupling between the two inner resonators. When α is equal to 0 or 4, the first-order inward hierarchical metamaterial is again reduced to a zeroth-order metamaterial inducing one band gap at lower frequencies. The band gap frequencies of the metamaterial with $\alpha = 4$ is lower than that with $\alpha = 0$, which is caused by the fact that the stacked springs reduce the effective stiffness. As also shown in the three figures, when α gradually increases from 0 to 4, the blue region gradually shifts to lower frequencies accompanying a slight bandwidth change, whereas the red region drops from higher frequencies and then jumps back to higher frequencies and the bandwidth is broader at lower frequencies than that at higher frequencies. By comparing the three figures, when the stiffness ratio $k_1^{(I)}/k_2^{(I)}$ decreases, the bandwidths of high-frequency band gaps (red regions) decreases significantly and is nearly neglectable for the case shown in Fig. 4(f). In contrast with outward metamaterials, the inward metamaterials demonstrate much better wave attenuation performances at relatively lower frequencies. Nonetheless, the parallel resonator design in the outward metamaterial can produce much broader band gaps at relatively higher-frequencies.

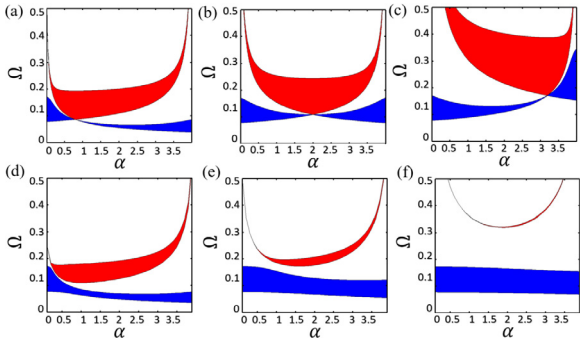

Fig. 4. System parameters are, $\alpha = m_1/m_0$ $m_1 + m_2 = 4m_0$ and $k_2/k_0 = 4/30$ $k_0/m_0 = 5e^8$, $\omega_0 = 2.2364$ (a) Bandgap of outward HHM for first-order when $k_1 = 4k_2 = 16/30k_0$, (b) bandgap of outward HHM for first-order when $k_1 = k_2 = 4/30k_0$, (c) bandgap of outward HHM for 1st order when $k_1 = 0.25k_2 = 1/30k_0$, (d) bandgap of inward HHM for first-order when $k_1 = 4k_2 = 16/30k_0$, (e) bandgap of inward HHM for first-order when $k_1 = k_2 = 4/30k_0$, (f) bandgap of inward HHM for first-order when $k_1 = 0.25k_2 = 1/30k_0$.

3. A honeycomb hierarchical lattice metamaterial with embedded local resonators

Lattice metamaterials with embedded resonators have been extensively studied for vibration suppression at sub-wavelength scales [26], due to their light-weight and broad implications in various engineering applications. Here, the design concept of hierarchical metamaterials demonstrated in Sec. 2 is implemented into a honeycomb hierarchical lattice with embedded resonators. Without loss of generality, we design and numerically as well as experimentally demonstrate an outward honeycomb hierarchical first-order lattice metamaterial for vibration suppression at desired frequencies.

3.1. Design of the outward honeycomb hierarchical lattice metamaterial

Fig. 5(a) shows the regular (zeroth-order hierarchy) honeycomb lattice structure, where the hexagonal edge length is denoted as L_B, and the width of each edge in the lattice is represented by t_0. The first-order hierarchical honeycomb lattice, which is schematically shown in Fig. 5(b), is constructed by expanding each node on the regular honeycomb lattice to a subsequent hexagonal lattice connected with the original one, where the edge width becomes t_1 to maintain the same mass density with the zeroth-order lattice. As shown in the figure, the edge length of the subsequent hexagonal lattice is denoted as L_1. It should be mentioned that this newly formed hierarchical honeycomb lattice can possess an extremely low percentage of the total mass of a bulk material occupying the same area in the plane of the lattice.

The hierarchical metamaterial lattice is then designed by filling the hexagonal voided areas with embedded local resonators periodically. As shown in Fig. 5(c), the zeroth-order metamaterial is composed by partially embedding lead cylinders with rubber coatings into the voided areas of a zeroth-order hierarchical honeycomb lattice. In the design, the lattice constant is selected as $2L_B$, and the radius of the lead cylinder is r_0. Similarly, the first order metamaterial is constructed with embedded lead cylinders with rubber coatings in both zeroth- and first-order hexagonal voided areas shown in Fig. 5(d). Here, the radius of the first-order lead cylinder is denoted as r_1. It should be noted that, by changing r_0 and r_1, the resonant frequencies of the zeroth- and first-order resonators can be independently tailored, inducing band gaps in different frequency regions.

3.2. Numerical simulations of the hierarchical lattices

The finite element method, with the commercial software COMSOL Multiphysics, is employed in the following studies to investigate the wave dispersion relations and vibration suppression performance of the honeycomb hierarchical

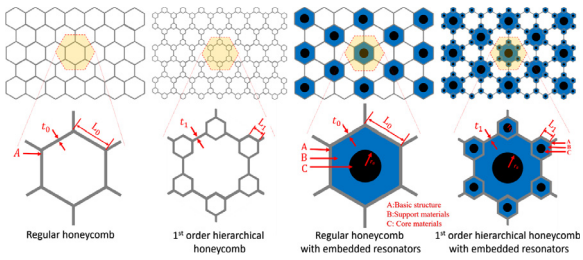

Fig. 5. Hierarchical Honeycomb Metamaterials with unit cells highlighted for: regular honeycomb; first order hierarchical honeycomb; regular honeycomb with embedded resonators; first order hierarchical honeycomb with embedded resonators.

metamaterial. This numerical approach is implemented due to the complex geometries and boundary conditions in the metamaterial structure which make it difficult to obtain analytical solutions. Fig. 6 shows the unit cell structure of the two honeycomb configurations with and without resonators given in Fig. 5. It should be mentioned that, in the numerical band gap calculations, the same reciprocal lattice vector is adopted for the honeycomb lattice with and without resonators, as a result, the reciprocal lattice vector is not irreducible for the two pure honeycomb lattices, and the corresponding band structures are not in the first Brillouin zone.

By prescribing periodic boundary conditions on the unit cell structures shown in Fig. 6, the dispersion diagrams are obtained for all of the four different configurations and shown in Fig. 7. In the numerical simulations, plane stress assumptions are used and the thickness of the lattice is selected as 10 mm. Free triangular elements are selected for all domains, and a direct eigenvalue solver (MUMPS) from COMSOL Multiphysics is used [59]. Material and geometric parameters of the lattice metamaterials are given in Table 1. It is worth mentioning that the first-order hierarchical honeycomb lattice only retains around 7% of the total mass of the homogeneous bulk material, and the first order hierarchical honeycomb lattice with resonators is almost 50% of its original total weight without voids. As shown in Fig. 7(a), for the zeroth-order honeycomb lattice, a complete band gap is clearly observed from 31200 to 37300 Hz, where all the wave modes incident from any directions are attenuated. By increasing the hierarchical order to one (Fig. 7(b)), this complete band gap is shifted to lower frequencies (14420–19800 Hz). Although the hierarchical order can be further increased to tailor the complete bandgap to much lower frequencies, this will produce complexities in the geometries and thus fabrication. To address this issue, hierarchically organized local resonators are periodically embedded in the voided areas, as the dispersion relations show in

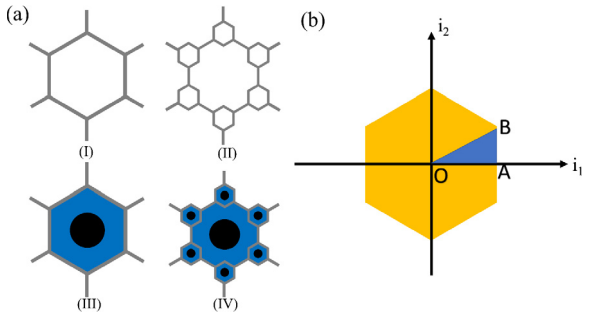

Fig. 6. (a) Unit cells selection (I) regular structure, (II) first-order hierarchical structure, (III) regular structure with embedded resonator, (IV) first-order hierarchical structure with embedded resonators. (b) The reciprocal lattice.

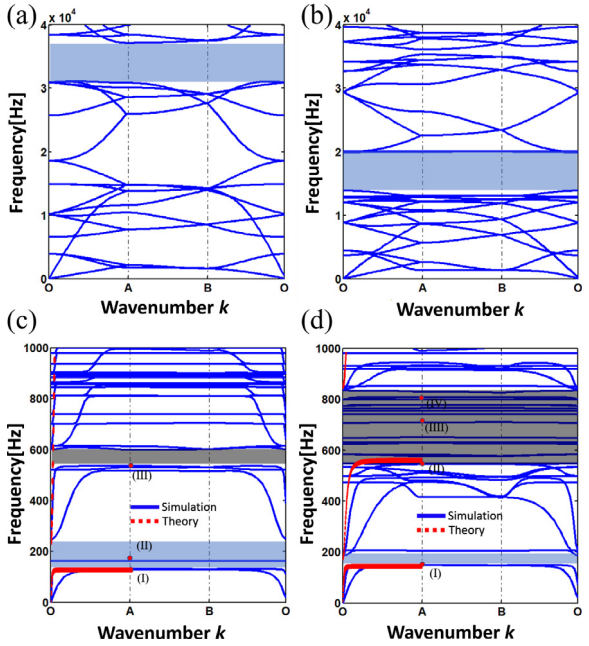

Fig. 7. (a) Dispersion relations of a regular honeycomb lattice; (b) Dispersion relations of a first-order hierarchical honeycomb lattice; (c) Dispersion relations of a regular honeycomb lattice embedded with resonators; (d) Dispersion relations of the hierarchical honeycomb lattice embedded with resonators.

Fig. 7(c) and (d), for zeroth- and first-order metamaterials, respectively. In Fig. 7(c), two separate band gaps are produced by the introduction of the zeroth-order resonators for both pressure and shear wave modes in extremely subwavelength frequency regions: 128–246 Hz and 529–600 Hz. The low-frequency band gap (128–246 Hz) is caused by the out-of-phase motion of the lead cylinders, where the mode shapes are shown in Fig. 8(a) and (b) (refer to the point denoted by "I" in Fig. 7(c)) for shear and pressure waves, respectively. The color bar in Fig. 8 denotes the absolute value of the total displacement ($||u|| + ||v||$), and arrows represent the displacement vectors. It is also interesting to note that a very narrow pass band appears within this band gap at 529 Hz. By looking at the mode shape in Fig. 8(c) (refer to the point denoted by "II" in Fig. 7(c)), we find this pass band is caused by the rotational motion of the lead cylinder. Furthermore, for the high-frequency band gap (529–600 Hz), it can be found from Fig. 8(d) and (e) that the out-of-phase resonant motion of the rubber coating layer contributes primarily to this gap for either pressure or shear waves (refer to the point denoted by "III" in Fig. 7(c)). The band structure of the first-order hierarchical metamaterial is shown in Fig. 7(d), where the two band gaps are still found in the frequency regions of 146–186 Hz and 546–840 Hz. Comparing with Fig. 7(c), the low-frequency band gap becomes narrower, whereas the high-frequency band gap becomes super-broad. It should be mentioned that the previous pass band in the low-frequency band gap (Fig. 7(c)) is removed in Fig. 7(d). Whereas, the working mechanism for this low-frequency band gap is the same as those of the zeroth-order metamaterial, as shown in the mode shapes shown in Fig. 9(a) and (b) (refer to the point denoted by "I" in Fig. 7(d)). However, the super-broad high-frequency band gap is mainly caused by the resonant motions of the first-order resonators (Fig. 9(c) and (d) (refer to the point denoted by "II" in Fig. 7(d))), where several pass bands are also found, due to the higher order resonances of the rubber layer as the mode shapes show in Fig. 9(e) and (f) (refer to the points denoted by "III" and "IV", respectively, in Fig. 7(d)).

In Fig. 7(c) and (d), we also apply the analytical model presented in Sec. 2 to calculate band structures of the honeycomb lattice metamaterials and compared with numerical simulations for waves propagated along one direction (red dotted curves). In the study, the aluminum honeycomb lattice is simplified as a linear mass-spring system with $m_0 = 9L_0t_0\rho_A$ and $k_0 = (E_At_0^3)/(2L_0^3)$, where the mass and spring constant are obtained from the first cutoff frequency of the connected beam [58,59]. The regular lead-rubber core is represented by an inner mass-spring resonator with $m_1 = \pi r_0^2\rho_C$ and $k_1 = (3E_BL_0b)/(2(L_0 - r_0))$, and the first-order lead-rubber core is modelled as an inner mass-spring resonator with $m_2 = 6\pi r_1^2\rho_C$ and $k_2 = 6(3E_BL_1b)/(2(L_1 - r_1))$. Note that only the longitudinal mode is considered in analytical calculations. It can be clearly seen from Fig. 7(c) and (d) that analytical results have a reasonable agreement with numerical ones for both regular (Fig. 7(c)) and hierarchical honeycomb lattice metamaterials (Fig. 7(d)). Although the full dispersion relations cannot be predicted by the analytical model, the results demonstrated in Sec. 2 provide a quick prediction of locally resonant band gaps, especially for bandwidths and frequency locations.

Table 1
Geometrical and material parameters of the hierarchical metamaterial.

Geometrical parameters		Material parameters		
Regular structure	$t_0 = 1.6\ mm$	Basic structure: Aluminum	Mass density	2700 $kg \cdot m^{-3}$
	$L_0 = 24\ mm$		Young's modulus	71 *GPa*
	$r_0 = 10.3\ mm$		Poisson's ratio	0.33
First order hierarchical structure	$t_1 = 1\ mm$	Support material:	Mass density	1340 $kg \cdot m^{-3}$
	$L_1 = 6\ mm$	Silicon rubber	Young's modulus	0.4 *MPa*
	$r_0 = 7.3\ mm$		Poisson's ratio	0.47
Thickness	$r_1 = 3\ mm$	Core material:	Mass density	11340 $kg \cdot m^{-3}$
	$b = 10\ mm$	Lead	Young's modulus	160 *GPa*
			Poisson's ratio	0.44

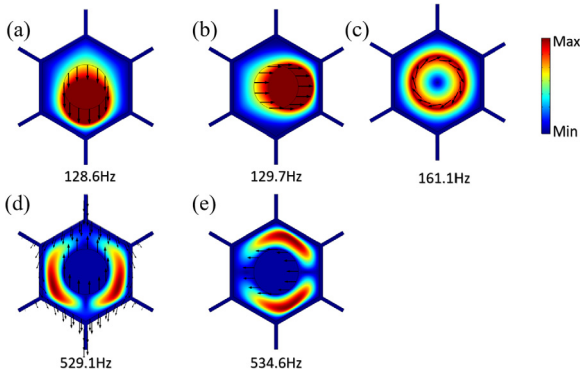

Fig. 8. Mode shapes of regular structure with embedded resonator: (a) 128.6 Hz, (b) 129.7 Hz, (c) 161.1 Hz, (d) 529.1 Hz, (e) 534.6 Hz.

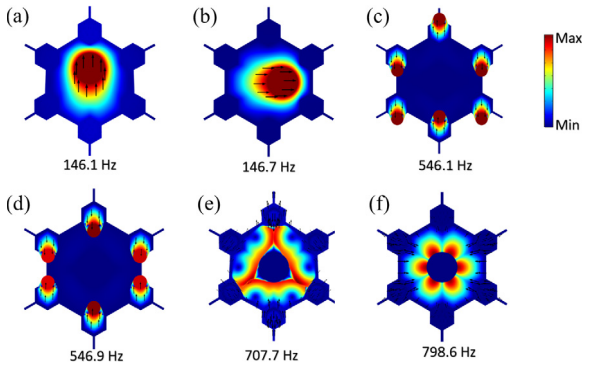

Fig. 9. Mode shape of first-order hierarchical structure with embedded resonators: (a) 146.1 Hz, (b) 146.7 Hz, (c) 546.1 Hz, (d) 546.9 Hz, (e) 707.7 Hz, (f) 798.6 Hz.

This super-broadband gap together with the narrow bandgap at lower frequencies are then examined by conducting numerical vibration simulations of the frequency response of a first-order hierarchical metamaterial with 11 unit cells, as schematically shown in Fig. 10(a). In the study, the left edge of the metamaterial is fixed and a point force excitation is applied on the bottom boundary of the metamaterial near the fixed edge. The damping parameter of the rubber is properly considered with a loss factor being $1 \times 10^{-5}s$. Fig. 10(b) shows the frequency response function of this first-order honeycomb lattice with and without resonators. In the figure, two response dips (red solid curve, 146–186 Hz and 546–840 Hz) for the lattice with resonators are clearly seen in comparison with the lattice without resonators (black dashed curve). It is also found that the two vibration suppression frequency regions (shaded areas) agree well with the band gap frequencies in the dispersion relations shown in Fig. 7(d). The vibration mode shapes demonstrated in Fig. 10(c) and (d) at 146 and 546 Hz, respectively, show the efficiency of the design. Only 5 layers of the metamaterial could produce strong vibration suppression.

3.3. *Experimental validations of the first-order outward hierarchical metamaterial*

To further validate the design, vibration tests of the first-order outward hierarchical lattice metamaterial are conducted. Fig. 11 shows the overview of the experimental setup. In the experiment, the honeycomb lattice is fabricated by cutting periodic hexagonal voids from an aluminum plate using a waterjet cutting machine. The final lattice structure is designed to contain 13 zeroth-order hexagonal voids over its length and three zeroth-order hexagonal voids in the height direction. The geometric parameters of the lattice are the same as those used in the numerical simulations, which are given in Table 1. The embedded resonators are implanted into the hierarchical honeycomb lattice by using a custom made mold. As shown in Fig. 11, the lower edge of the sample is fixed, and the excitation force is applied by a shaker (LDS V203) driven by a power amplifier (LDS PA25E) connected to the sample near the fixed end. In the numerical and experimental setup, harmonic loadings are applied. Thus, no propagating wave exists in the structure; only standing waves appear. Aligning the accelerometer with the shaker along the vertical direction provides similar responses as those used in the current numerical and experimental setup. A white noise excitation signal with frequencies from 0 to 1000 Hz is used and the vibration response is captured with an accelerometer fixed to the other end of the lattice. The input and output signals are recorded with a dynamic

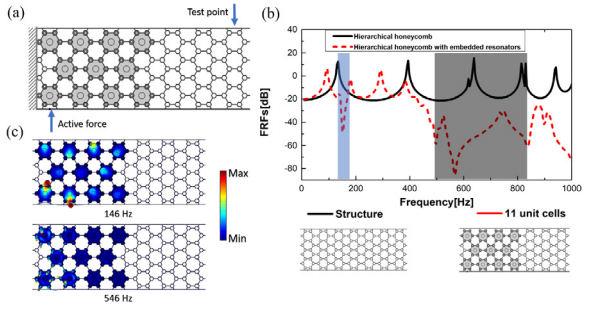

Fig. 10. (a) Schematic of numerical simulations for FRF calculations. A point force along the vertical direction is applied at the bottom of the structure near the fixed edge and the displacement response is obtained at the top of the structure near the free edge; (b) Simulated FRF of the hierarchical honeycomb lattice metamaterial with 11 unit cells. The blue and gray shaded areas denote the first and second bandgaps calculated from dispersion relations (Fig. 7), respectively. (c) Mode shapes of the hierarchical honeycomb lattice metamaterial at 146 Hz and 546 Hz, respectively.

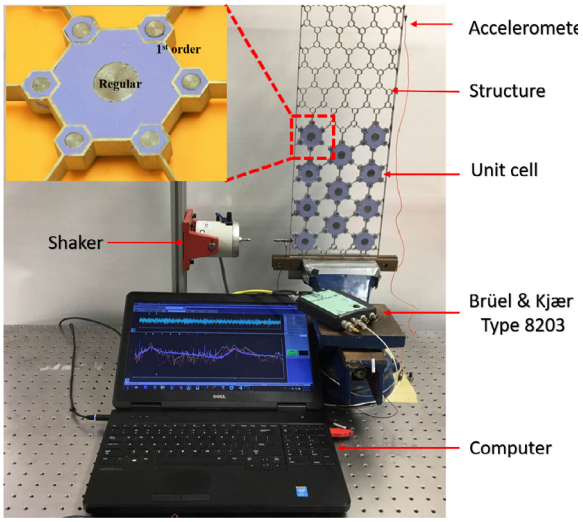

Fig. 11. Experimental set-up of the vibration testing of the HHM beam. The HHM beam is fixed in the vertical direction at the bottom, and the gray material is aluminum, the purple material is rubber and the deep gray material is lead.

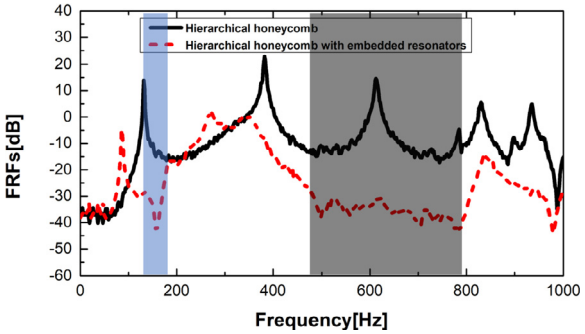

Fig. 12. Experimentally measured FRF of the hierarchical honeycomb lattice metamaterial with 11 unit cells. The blue and gray shaded areas denote the first and second bandgaps calculated from dispersion relations (Fig. 7), respectively.

signal analyzer via a PC-interface (Brüel & Kjær Type 8203). Fig. 12 shows the experimentally measured frequency response function of the first-order honeycomb lattice with and without resonators. The expected response dips in the frequency regions, 144–188 Hz and 480–810 Hz is clearly seen, which also have a reasonable agreement with the numerical simulations shown in Fig. 10.

4. Conclusions

In this paper, we suggest a hierarchical metamaterial with local resonators to tailor the band gaps with different frequency regions at subwavelength scales. An analytical model is proposed to investigate the dispersion relations of a one-dimensional hierarchical lumped mass-spring metamaterial. We quantitatively examine band gap variations with different mass and stiffness ratios for the resonators with both inward and outward configurations. Based on the results from the analytical model, a first-order honeycomb outward hierarchical lattice metamaterial is then designed for vibration suppression at two separate desired frequency bands. Both numerical and experimental approaches are implemented and good agreement have been found to illustrate the vibration attenuation efficiency of the current design. It is our hope that the hierarchical metamaterials could be an efficient solution in vibration and/or elastic wave control engineering at subwavelength scales.

Acknowledgments

This work is supported by the Air Force Office of Scientific Research under Grant No. AF 9550-18-1-0096 with Program Manager Dr. Byung-Lip (Les) Lee.

References

[1] J.B. Pendry, Negative refraction makes a perfect lens, Phys. Rev. Lett. 85 (18) (2000) 3966.
[2] T. Tanaka, A. Ishikawa, S. Kawata, Unattenuated light transmission through the interface between two materials with different indices of refraction using magnetic metamaterials, Phys. Rev. B 73 (12) (2006) 125423.
[3] W. Cai, V. Shalaev, Optical Metamaterials: Fundamentals and Applications, Springer Science & Business Media, 2009.
[4] P.A. Deymier (Ed.), Acoustic Metamaterials and Phononic Crystals, vol. 173, Springer Science & Business Media, 2013.
[5] M.I. Hussein, M.J. Leamy, M. Ruzzene, Dynamics of phononic materials and structures: historical origins, recent progress, and future outlook, Appl. Mech. Rev. 66 (4) (2014) 040802.
[6] J. Li, C.T. Chan, Double-negative acoustic metamaterial, Phys. Rev. 70 (5) (2004) 055602.
[7] N. Fang, H. Lee, C. Sun, X. Zhang, Sub–diffraction-limited optical imaging with a silver superlens, Science 308 (5721) (2005) 534–537.
[8] X. Xu, P. Li, X. Zhou, G. Hu, Experimental study on acoustic subwavelength imaging based on zero-mass metamaterials, EPL (Europhy. Lett.) 109 (2) (2015) 28001.
[9] Z. Yang, J. Mei, M. Yang, N.H. Chan, P. Sheng, Membrane-type acoustic metamaterial with negative dynamic mass, Phys. Rev. Lett. 101 (20) (2008) 204301.
[10] J. Mei, G. Ma, M. Yang, Z. Yang, W. Wen, P. Sheng, Dark acoustic metamaterials as super absorbers for low-frequency sound, Nat. Commun. 3 (2012) 756.
[11] Y. Chen, G. Huang, X. Zhou, G. Hu, C.T. Sun, Analytical coupled vibroacoustic modeling of membrane-type acoustic metamaterials: membrane model, J. Acoust. Soc. Am. 136 (3) (2014) 969–979.
[12] Z. Liu, X. Zhang, Y. Mao, Y.Y. Zhu, Z. Yang, C.T. Chan, P. Sheng, Locally resonant sonic materials, Science 289 (5485) (2000) 1734–1736.
[13] S. Yao, X. Zhou, G. Hu, Experimental study on negative effective mass in a 1D mass–spring system, New J. Phys. 10 (4) (2008) 043020.
[14] H.H. Huang, C.T. Sun, G.L. Huang, On the negative effective mass density in acoustic metamaterials, Int. J. Eng. Sci. 47 (4) (2009) 610–617.
[15] Y. Lai, Y. Wu, P. Sheng, Z.Q. Zhang, Hybrid elastic solids, Nat. Mater. 10 (8) (2011) 620.
[16] X.N. Liu, G.K. Hu, G.L. Huang, C.T. Sun, An elastic metamaterial with simultaneously negative mass density and bulk modulus, Appl. Phys. Lett. 98 (25) (2011) 251907.
[17] R. Zhu, X.N. Liu, G.K. Hu, C.T. Sun, G.L. Huang, Negative refraction of elastic waves at the deep-subwavelength scale in a single-phase metamaterial, Nat. Commun. 5 (2014) 5510.
[18] G.L. Huang, C.T. Sun, Band gaps in a multiresonator acoustic metamaterial, J. Vib. Acoust. 132 (3) (2010) 031003.
[19] K.T. Tan, H.H. Huang, C.T. Sun, Blast-wave impact mitigation using negative effective mass density concept of elastic metamaterials, Int. J. Impact Eng. 64 (2014) 20–29.
[20] R.V. Craster, S. Guenneau (Eds.), Acoustic Metamaterials: Negative Refraction, Imaging, Lensing and cloaking, vol. 166, Springer Science & Business Media, 2012.
[21] M. Molerón, C. Daraio, Acoustic metamaterial for subwavelength edge detection, Nat. Commun. 6 (2015) 8037.
[22] R. Zhu, X.N. Liu, G.K. Hu, C.T. Sun, G.L. Huang, A chiral elastic metamaterial beam for broadband vibration suppression, J. Sound Vib. 333 (10) (2014) 2759–2773.
[23] M.I. Hussein, M.J. Frazier, Metadamping: an emergent phenomenon in dissipative metamaterials, J. Sound Vib. 332 (20) (2013) 4767–4774.
[24] M. Miniaci, A.S. Gliozzi, B. Morvan, A. Krushynska, F. Bosia, M. Scalerandi, N.M. Pugno, Proof of concept for an ultrasensitive technique to detect and localize sources of elastic nonlinearity using phononic crystals, Phys. Rev. Lett. 118 (21) (2017) 214301.
[25] J.M. Manimala, C.T. Sun, Microstructural design studies for locally dissipative acoustic metamaterials, J. Appl. Phys. 115 (2) (2014) 023518.
[26] P.F. Pai, H. Peng, S. Jiang, Acoustic metamaterial beams based on multi-frequency vibration absorbers, Int. J. Mech. Sci. 79 (2014) 195–205.
[27] Z. Su, W. Peng, Z. Zhang, G. Gogos, R. Skaggs, B. Cheeseman, Numerical simulation of a novel blast wave mitigation device, Int. J. Impact Eng. 35 (5) (2008) 336–346.
[28] X.N. Liu, G.K. Hu, C.T. Sun, G.L. Huang, Wave propagation characterization and design of two-dimensional elastic chiral metacomposite, J. Sound Vib. 330 (11) (2011) 2536–2553.
[29] Y.Y. Chen, M.V. Barnhart, J.K. Chen, G.K. Hu, C.T. Sun, G.L. Huang, Dissipative elastic metamaterials for broadband wave mitigation at subwavelength scale, Compos. Struct. 136 (2016) 358–371.
[30] Y.Y. Chen, G.L. Huang, C.T. Sun, Band gap control in an active elastic metamaterial with negative capacitance piezoelectric shunting, J. Vib. Acoust. 136 (6) (2014) 061008.
[31] N. Kherraz, L. Haumesser, F. Levassort, P. Benard, B. Morvan, Controlling Bragg gaps induced by electric boundary conditions in phononic piezoelectric plates, Appl. Phys. Lett. 108 (9) (2016) 093503.
[32] F. Casadei, T. Delpero, A. Bergamini, P. Ermanni, M. Ruzzene, Piezoelectric resonator arrays for tunable acoustic waveguides and metamaterials, J. Appl. Phys. 112 (6) (2012) 064902.
[33] A. Bergamini, T. Delpero, L.D. Simoni, L.D. Lillo, M. Ruzzene, P. Ermanni, Phononic crystal with adaptive connectivity, Adv. Mater. 26 (9) (2014) 1343–1347.
[34] Y.Y. Chen, G.K. Hu, G.L. Huang, An adaptive metamaterial beam with hybrid shunting circuits for extremely broadband control of flexural waves, Smart Mater. Struct. 25 (10) (2016) 105036.
[35] Y.Y. Chen, R. Zhu, M.V. Barnhart, G.L. Huang, Enhanced flexural wave sensing by adaptive gradient-index metamaterials, Sci. Rep. 6 (2016) 35048.
[36] R. Zhu, Y.Y. Chen, M.V. Barnhart, G.K. Hu, C.T. Sun, G.L. Huang, Experimental study of an adaptive elastic metamaterial controlled by electric circuits, Appl. Phys. Lett. 108 (1) (2016) 011905.
[37] Y. Chen, X. Li, H. Nassar, G.K. Hu, G. Huang, A programmable metasurface for real time control of broadband elastic rays, Smart Mater. Struct. 27 (11) (2018) 115011.
[38] X. Li, Y. Chen, G. Hu, G. Huang, A self-adaptive metamaterial beam with digitally controlled resonators for subwavelength broadband flexural wave attenuation, Smart Mater. Struct. 27 (4) (2018) 045015.
[39] A. Ajdari, B.H. Jahromi, J. Papadopoulos, H. Nayeb-Hashemi, A. Vaziri, Hierarchical honeycombs with tailorable properties, Int. J. Solid Struct. 49 (11–12) (2012) 1413–1419.
[40] K. Bertoldi, Harnessing instabilities to design tunable architected cellular materials, Annu. Rev. Mater. Res. 47 (2017) 51–61.
[41] D. Rayneau-Kirkhope, Y. Mao, R. Farr, Ultralight fractal structures from hollow tubes, Phys. Rev. Lett. 109 (20) (2012) 204301.
[42] E.M. Arndt, W. Moore, W.K. Lee, C. Ortiz, Mechanistic origins of bombardier beetle (Brachinini) explosion-induced defensive spray pulsation, Science 348 (6234) (2015) 563–567.
[43] D.J. Bodony, L. Day, A.R. Friscia, L. Fusani, A. Karon, G.W. Swenson, M. Wikelski, B.A. Schlinger, Determination of the wingsnap sonation mechanism of the golden-collared manakin (Manacus vitellinus), J. Exp. Biol. 219 (10) (2016) 1524–1534.
[44] R. Oftadeh, B. Haghpanah, D. Vella, A. Boudaoud, A. Vaziri, Optimal fractal-like hierarchical honeycombs, Phys. Rev. Lett. 113 (10) (2014) 104301.
[45] F. Song, J. Zhou, X. Xu, Y. Xu, Y. Bai, Effect of a negative Poisson ratio in the tension of ceramics, Phys. Rev. Lett. 100 (24) (2008) 245502.
[46] R. Gatt, L. Mizzi, J.I. Azzopardi, K.M. Azzopardi, D. Attard, A. Casha, J. Briffa, J.N. Grima, Hierarchical auxetic mechanical metamaterials, Sci. Rep. 5 (2015) 8395.
[47] P. Zhang, A.C. To, Broadband wave filtering of bioinspired hierarchical phononic crystal, Appl. Phys. Lett. 102 (12) (2013) 121910.
[48] Q.J. Lim, P. Wang, S.J.A. Koh, E.H. Khoo, K. Bertoldi, Wave propagation in fractal-inspired self-similar beam lattices, Appl. Phys. Lett. 107 (22) (2015) 221911.

[49] D. Mousanezhad, S. Babaee, R. Ghosh, E. Mahdi, K. Bertoldi, A. Vaziri, Honeycomb phononic crystals with self-similar hierarchy, Phys. Rev. B 92 (10) (2015) 104304.
[50] Q.J. Lim, P. Wang, S.J.A. Koh, E.H. Khoo, K. Bertoldi, Wave propagation in fractal-inspired self-similar beam lattices, Appl. Phys. Lett. 107 (22) (2015) 221911.
[51] Y. Chen, L. Wang, Harnessing structural hierarchy to design stiff and lightweight phononic crystals, Extr. Mech. Lett. 9 (2016) 91–96.
[52] J. Liu, L. Li, B. Xia, X. Man, Fractal labyrinthine acoustic metamaterial in planar lattices, Int. J. Solid Struct. 132 (2018) 20–30.
[53] C. Liu, C. Reina, Broadband locally resonant metamaterials with graded hierarchical architecture, J. Appl. Phys. 123 (9) (2018) 095108.
[54] M. Miniaci, A. Krushynska, A.S. Gliozzi, N. Kherraz, F. Bosia, N.M. Pugno, Design and fabrication of bioinspired hierarchical dissipative elastic metamaterials, Phys. Rev. Appl. 10 (2) (2018) 024012.
[55] M. Miniaci, A. Krushynska, A.B. Movchan, F. Bosia, N.M. Pugno, Spider web-inspired acoustic metamaterials, Appl. Phys. Lett. 109 (7) (2016) 071905.
[56] R.U. Ahmed, S. Banerjee, Wave propagation in metamaterial using multiscale resonators by creating local anisotropy, Int. J. Mod. Eng. 13 (2) (2013) 51.
[57] V. Romero-García, A. Krynkin, L.M. Garcia-Raffi, O. Umnova, J.V. Sánchez-Pérez, Multi-resonant scatterers in sonic crystals: locally multi-resonant acoustic metamaterial, J. Sound Vib. 332 (1) (2013) 184–198.
[58] A.S. Phani, J. Woodhouse, N.A. Fleck, Wave propagation in two-dimensional periodic lattices, J. Acoust. Soc. Am. 119 (4) (2006) 1995–2005.
[59] M.V. Barnhfart, X. Xu, Y. Chen, S. Zhang, J. Song, G. Huang, Experimental demonstration of a dissipative multi-resonator metamaterial for broadband elastic wave attenuation, J. Sound Vib. 438 (2019) 1–12.